ELSEVIER

Journal of Nuclear Materials 265 (1999) 273–284

journal of nuclear materials

Accumulation of radioactive corrosion products on steel surfaces of VVER type nuclear reactors. I. ^{110m}Ag

Gábor Hirschberg [a], Pál Baradlai [a], Kálmán Varga [a,*], Gerrit Myburg [b], János Schunk [c], Péter Tilky [c], Paul Stoddart [d]

[a] *Department of Radiochemistry, University of Veszprém, PO Box 158, 8201 Veszprém, Hungary*
[b] *Department of Physics, University of Pretoria, Pretoria, South Africa*
[c] *Paks NPP Co. Ltd., Paks, Hungary*
[d] *MATTEK, CSIR, Box 395, Pretoria, South Africa*

Received 3 August 1998; accepted 20 October 1998

Abstract

Formation, presence and deposition of corrosion product radionuclides (such as ^{60}Co, ^{51}Cr, ^{54}Mn, ^{59}Fe and/or ^{110m}Ag) in the primary circuits of water-cooled nuclear reactors (PWRs) throw many obstacles in the way of normal operation. During the course of the work presented in this series, accumulations of such radionuclides have been studied at austenitic stainless steel type 08X18H10T (GOST 5632-61) surfaces (this austenitic stainless steel corresponds to AISI 321). Comparative experiments have been performed on magnetite-covered carbon steel (both materials are frequently used in some Soviet VVER type PWRs). For these laboratory-scale investigations a combination of the in situ radiotracer 'thin gap' method and voltammetry is considered to be a powerful tool due to its high sensitivity towards the detection of the submonolayer coverages of corrosion product radionuclides. An independent technique (XPS) is also used to characterize the depth distribution and chemical state of various contaminants in the passive layer formed on austenitic stainless steel. In the first part of the series the accumulation of ^{110m}Ag has been investigated. Potential dependent sorption of Ag^+ ions (cementation) is found to be the predominant process on austenitic steel, while in the case of magnetite-covered carbon steel the silver species are mainly depleted in the form of Ag_2O. The XPS depth profile of Ag gives an evidence about the embedding of metallic silver into the entire passive layer of the austenitic stainless steel studied.

PACS: 82.55.+e; 81.65.Kn; 79.60.Ht

1. Introduction

The knowledge of the state and sorption behavior of corrosion products adhered to the steel surfaces in cooling circuits of water-cooled nuclear reactors is of great importance for a number of practical reasons. For instance, under normal operating conditions (when there is no fission product release due to fuel cladding failure) the majority of radioactive contamination in the primary circuit is caused by various radioactive corrosion products (see Refs. [1–7] and references cited therein). These corrosion products are dissolved from construction materials, activated in the reactor core, and redeposited onto the surfaces of primary cooling circuit. The most important corrosion product radionuclides in the primary side coolant of pressurized water reactors (PWRs) are ^{60}Co, ^{58}Co, ^{110m}Ag, ^{51}Cr, ^{54}Mn, ^{59}Fe [1–7]. The two cobalt isotopes are known to be the predominant contaminants, but the ^{110m}Ag radionuclide (originating from the welding material of some Soviet VVER-type PWRs) may also contribute significantly to the radiation exposure of the operating personnel. Moreover, the many γ-photons of different energy emitted by ^{110m}Ag (see Table 1) hinder the continuous detection of other solution contaminants, leading to troubles in the monitoring of e.g. fission product release (if any) [4–7].

* Corresponding author. Fax: +36-88 427 681; e-mail: vargakl@almos.vein.hu.

0022-3115/99/$ – see front matter
PII: S0022-3115(98)00656-4

Table 1
Energies and decay probabilities of particles emitted by ^{110m}Ag ($T_{1/2} = 249.85$ day)

$E_{\beta max}$ (MeV)	Probability (%)	E_γ (MeV)	Probability (%)	E_γ (MeV)	Probability (%)	E_γ (MeV)	Probability (%)
0.084	67.30	0.003	0.07	0.447	3.64	0.764	22.28
0.134	0.41	0.022	0.20	0.620	2.77	0.818	7.28
0.315	0.19	0.022	0.37	0.626	0.23	0.885	72.58
0.531	30.50	0.025	0.12	0.658	94.39	0.937	34.19
–	–	0.099	0.01	0.677	0.14	0.997	0.12
–	–	0.003	0.02	0.678	10.68	1.334	0.13
–	–	0.023	0.06	0.687	6.47	1.384	24.26
–	–	0.023	0.12	0.707	16.68	1.476	4.00
–	–	0.026	0.04	0.708	0.28	1.505	13.06
–	–	0.365	0.11	0.744	4.64	1.562	1.18

Therefore, it can easily be understood that knowledge of the fundamental aspects of ^{110m}Ag deposition is needed, which may facilitate the elaboration of more efficient surface prevention and/or decontamination procedures.

As demonstrated above, corrosion and contamination processes in the primary cooling circuit of PWRs are essentially interrelated: the contaminant isotopes are mostly corrosion products activated in the reactor core, and the contamination takes place on surfaces which were modified by the corrosion. Also, the two counter measures (decontamination and corrosion-prevention) are connected to each other by similar ways: the usual and effective decontamination methods cause a certain extent of corrosion, while a successful corrosion-prevention method can retard the contamination as well. Establishing the inevitable links between corrosion and contamination phenomena should lead to a new approach in handling the complex problems of contamination/decontamination and corrosion/corrosion-prevention. A schematic presentation of this approach is shown in Fig. 1, in which it is essential to emphasize the importance of the electrochemical aspects of contamination and decontamination. As also seen in Fig. 1, in response to the need for the better understanding of the kinetics and mechanism of above mentioned processes, the first step is the application of laboratory-scale measuring systems. The next step required is the investigation of the phenomena in simulated model systems. A careful inspection of the available literature data ([1–8] and references cited therein) reveals that a wide variety of the investigation methods (laboratory, semi-plant and standardized techniques) can be applied for the study of radioactive contamination–decontamination processes in solid/liquid heterogeneous systems (see Fig. 2).

The methods used on laboratory scale should be able to combine advantages of the experimental techniques of radiochemistry, electrochemistry and corrosion science to explain the relevant problems. Therefore, one has to choose investigation methods from the potentially great number of possibilities compiled in Fig. 2 that can answer most of the posing questions. Among these methods, simultaneous use (coupling) of in situ radiotracer (such as 'thin layer', 'foil' and 'electrode lowering' (thin gap)) and electrochemical techniques is considered to be one of the most powerful tools. The in situ techniques constitute a group of radiolabeling methods, which enables the continuous study of the surface excess concentration (radioactivity) of adsorbed species on the electrode surface immersed in a solution. All these methods utilize the thin layer principle, and seem to be the most advanced technical solutions for the investigation of interfacial phenomena in solid/liquid heterogeneous systems from both radiochemical and electrochemical points of view [8–12].

In the past decade two in situ radiotracer methods (namely the foil and the electrode lowering (thin gap) techniques) have been adopted and further developed in our laboratory ([8,13] and references cited therein). Recently, the progress in the methodology and technical solutions of our version of the thin gap method has reached a certain level [8,13–15], where the investigation

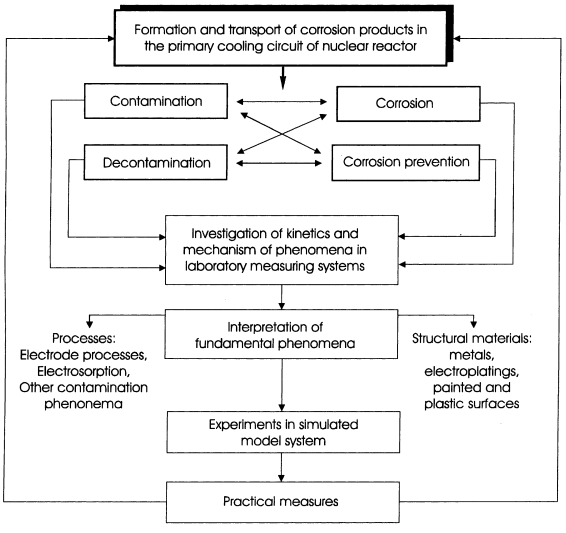

Fig. 1. The complex view of the study of contamination–decontamination, corrosion–corrosion prevention problems that occur in nuclear power plants.

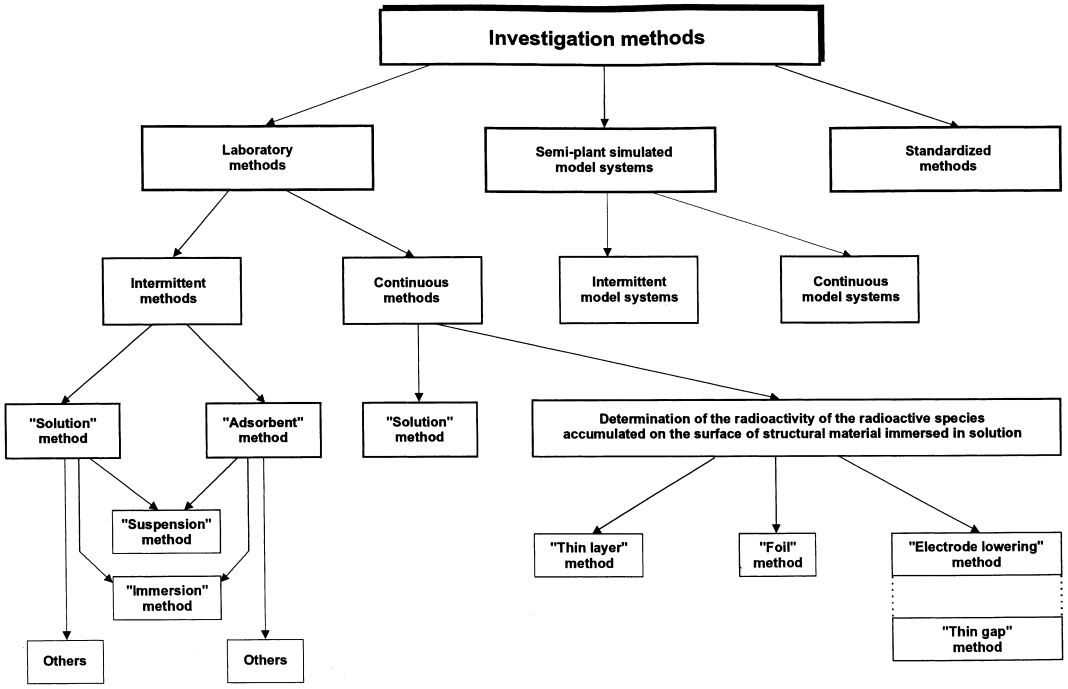

Fig. 2. Investigation methods used for the study of radioactive contamination–decontamination processes.

of corrosion and contamination processes on construction materials of industrial importance becomes possible. The aim of the present work is therefore to study the deposition of ^{110m}Ag on two steel surfaces (austenitic stainless steel type 08X18H10T (GOST 5632-61) and magnetite-covered carbon steel) by a combination of the in situ radiotracer thin gap method and voltammetry. (Austenitic stainless steel type 08X18H10T corresponds to AISI 321. The magnetite-covered carbon steel is chosen to be the subject of comparative studies in order to gain some insight into the possible role of the magnetite layer in the ^{110m}Ag accumulation.) An independent technique (XPS) is also used to characterize the distribution and chemical state of silver deposits in the passive layer formed on austenitic stainless steel. The results provide additional information on the kinetics and mechanism of the surface contamination caused by ^{110m}Ag in the primary side coolant of VVER type nuclear reactors.

2. Experimental section

2.1. Theoretical basis and instrumentation of the in situ radiotracer thin gap method

The electrode lowering technique was established in 1966, and later refined by Kazarinov et al. [9,16,17]. Since 1987, significant progress in the methodology and applicability of the 'electrode lowering' method has been made by Wieckowski and co-workers ([10,11] and references cited therein) with the so-called in situ thin gap radiotracer technique.

The main elements of an upgraded version of the thin gap method elaborated in our laboratory [8,13–15] are schematically depicted in Fig. 3 (part A: scheme of the experiments, part B: sketch of the radioelectrochemical cell, part C: the measuring system). As demonstrated by Fig. 3(A) and (B), central part of the measuring equipment is a glass–Teflon–steel cell, which is designed for simultaneous radiochemical and electrochemical measurements. The reference electrode is a so-called reference hydrogen electrode (RHE); the auxiliary electrode is of a noble metal like gold or platinum. Li–glass scintillators with a thickness varying between 0.2–4 mm are mounted into the ceramic bottom of the cell and polished to optical quality. For reference and auxiliary experiments 0.1–5 mm thick β-plastic scintillator as well as silicon semiconductor (type: AMPTEK XR-100T) detector can also be used.

The schematic of the experiments may be seen in Fig. 3(A). With the working electrode in the raised position, the sorption processes proceed under well-controlled electrochemical conditions, and simultaneously, the counting rate originating from the bulk solution (I_B) is measured. (Meanwhile voltammetric measurements can also be carried out.) By squeezing the suitably designed electrode down against the scintillator, the sorp-

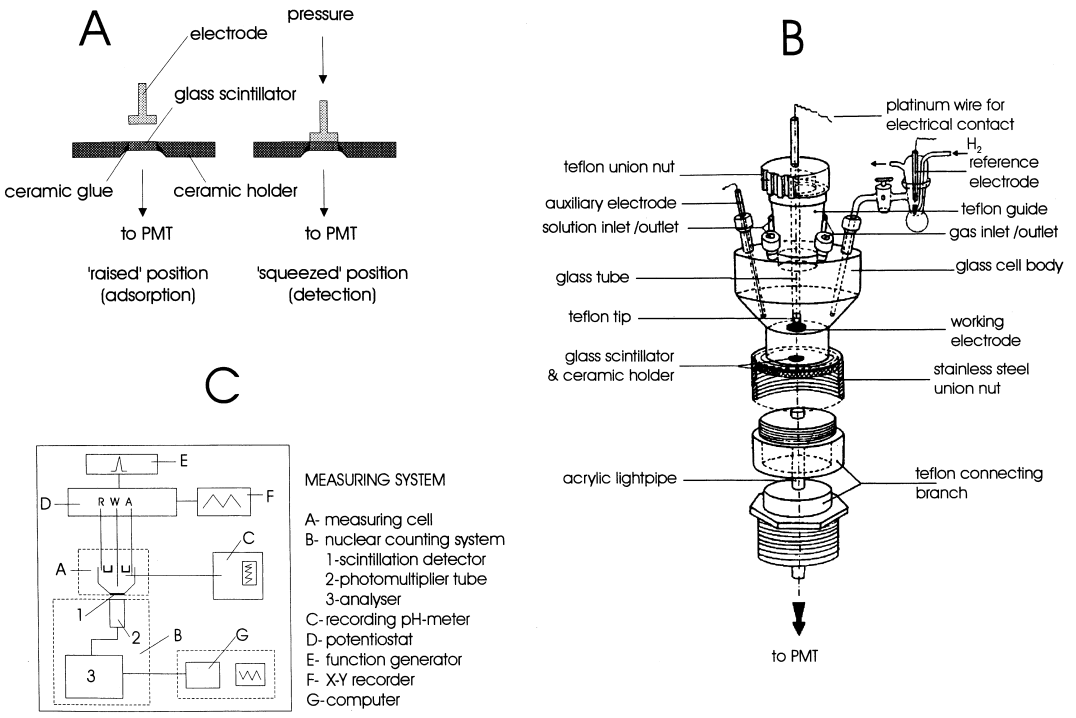

Fig. 3. The thin gap method. (A) Schematic of the experiments; (B) Simplified view of the radioelectrochemical cell; (C) Measuring system.

tion phenomena can be 'frozen up' and sum of the counting rate (I_A) proportional to the amount of species adsorbed on the working electrode and the counting rate coming from a thin solution gap ($d < 1$–2 μm) between the electrode and scintillator can be detected. With the present design of the thin gap method any species can be studied, if labeled with isotopes, that emit pure β-radiation of maximum energy ($E_{\beta max}$) higher than 67 keV ($H_2^{35}SO_4$, $H^{36}Cl$, organic and inorganic inhibitors labeled with ^{14}C, ^{35}S and ^{32}P etc.). Furthermore, the methodological developments make it possible to detect also β- and γ- (e.g. ^{110m}Ag, ^{60}Co [8,15,18–20]), as well as low energy ($E<20$ keV) γ- (X-ray) (e.g. ^{51}Cr, ^{55}Fe) emitting radioisotopes. A nuclear data processing system based on dual- and multichannel (8k) pulse-height analyzers and auxiliary electrochemical devices (Fig. 3(C)) enables one to characterize the surface structure and state via sorption processes.

In the present work, a special (so-called dE/dx) β-plastic scintillation detector (Thorn Emi, thickness: 100 μm) was applied for the in situ determination of the surface excess concentration (Γ) of Ag deposits labeled with ^{110m}Ag. The dE/dx detector made it possible to study the sorption phenomena via detection of β-particles emitted by ^{110m}Ag radionuclides (see Table 1). Disturbing effects of the secondary radiations (γ-ray, characteristic X-ray or bremsstrahlung, Compton- and photoelectrons) on the β detection were negligible or could be eliminated [8,15,18–20]. (We shall give an experimental evidence of the latter statement in the next Section 2.2.) At such conditions the Γ values of sorbed silver species were calculated by using the following relationship [10,11,15]

$$\Gamma = \frac{I_A c}{I_B \mu \gamma f_b \exp(-\mu x)}, \quad (1)$$

where c is the solution concentration (mol cm^{-3}), μ the linear attenuation coefficient for β-radiation of ^{110m}Ag measured in dilute water solution ($\mu = 36$ cm^{-1} [18]), f_b the measured value of the saturation backscattering factor ($f_{b,austenitic} = 1.21$; $f_{b,magn} = 1.30$), γ the roughness factor of the electrode surface (Owing to the lack of appropriate experimental method, the roughness factor could not be reliably measured. Therefore, we provide surface concentration data as a product of $\Gamma\gamma$) and x the actual thickness of solution gap. Other terms are as defined earlier.

2.2. Experimental set-up, procedures and chemicals

When the radioelectrochemical cell was assembled, the scintillator was attached to an acrylic light-pipe with silicon oil. The other end of the light-pipe was connected to the photocathode of a 16-dynode photomultiplier

tube (PMT). High voltage for the PMT was provided by a Thorn-EMI PM28B power supply unit. Signals from the photomultiplier tube were analyzed by an NK-350 (Gamma, Hungary) single channel analyzer (it recorded the gross intensity) and an NU 8110 (Merion EP, Hungary) 8k multichannel analyzer which produced pulse-height spectra. The measurements were carried out in a dark chamber. Potential control was applied via reference hydrogen and gold counter electrodes using an EF-435 type potentiostat, an EF-1808 function generator (both Elektroflex, Hungary) and a NE-244 type X–Y recorder (EMG, Hungary).

All the experiments were carried out at room temperature in a model solution of the primary cooling circuit of VVER type nuclear reactors. (The composition of this solution is tabulated in Table 2.) Disk-shaped electrodes (diameter: 10.0 mm; thickness: 2–3 mm) were cut from austenitic stainless steel type 08X18H10T (GOST 5632-61) and magnetite-covered carbon steel. The stainless steel samples were polished to optical quality with emery paper and diamond paste (down to 0.25 μm). The prepared electrodes were degreased with ethanol, washed with Millipore water and introduced to the cell. ^{110m}Ag was purchased from Amersham (specific activity: 6.8×10^{12} Bq/mol). All the reagents were analytical grade or Suprapure (Merck); solutions were prepared with ultrapure water (Millipore MilliQ^{50}). Potential values quoted in this paper are given on the RHE scale. Before and throughout the measurements the solution phase was purged and deoxygenated with argon gas (99.999 v/v%).

In addition, X-ray photoelectron spectroscopic (XPS) studies of austenitic stainless steel surfaces were carried out by a Quantum 2000 scanning ESCA microprobe. Al-K_α radiation with an energy of 1486.6 eV was used as primary X-ray source (set at 33 W) and an analysis area of about 200×200 μm^2. Sputtering was performed with 3 keV argon ions at a rate of about 1 nm/min (calibrated using Ta_2O_3 laser). For these measurements rectangular (20 mm × 20 mm) pieces of austenitic stainless steel type 08X18H10T were cut and polished with emery paper to a final grit No. 1200. The samples were degreased, washed and introduced to a conventional three-electrode electrochemical cell. At the end of the electrochemical measurement the samples were dried in vacuum for 3 h and packed into plastic containers (filled with high-purity argon to avoid contact with air) until loading into the spectrometer.

Table 2
The composition of the model solution ($pH_{25°C} \cong 7.7$)

Component	Concentration (g kg^{-1})
H_3BO_3	3
KOH	5.2×10^{-3}
NaOH	0.4×10^{-3}
LiOH	3.2×10^{-3}
NH_3	30×10^{-3}
N_2H_4	0.02×10^{-3}
O_2	$<0.02 \times 10^{-3}$
Cl^-, SO_4^{2-}	$<0.05 \times 10^{-3}$

3. Results and discussion

3.1. Voltammetric behavior of steel surfaces

Prior to the sorption experiments voltammetric measurements were performed to gain some insight into the passivation behavior of steel surfaces in model solution. Cyclic voltammograms of the two steel samples in the model solution of the primary circuit coolant are presented in Figs. 4 and 5.

Fig. 4(a) and (b) show the potential-window opening study of the austenitic stainless steel into positive and negative directions, respectively. The current–potential morphology of the voltammetric profiles is practically the same as that reported by Ramasubramanian et al. [21] and Wieckowski et al. [22] under very similar experimental conditions. From the voltammograms it is obvious that the austenitic stainless steel exhibits passive properties in a wide potential range (between −0.10 V and 1.10 V), including the corrosion potential. Polarizing the sample to more positive potential values (Fig. 4(a)) we experience two reduction peaks on the cathodic branch which are probably the results of the two-step reduction of species (Cr(VI) and Fe(III)) formed in the surface oxide in the region $E > 1.10$ V [21]. Upon sweeping down to potentials more negative than −0.10 V (Fig. 4(b)) a growing hump in the positive-going i–E curves at $E > 0$ V appears, which is likely related to the formation of iron oxides (i.e., active to passive transition) [21,22]. The most important conclusion to be drawn from the above voltammograms is that sorption experiments should only be carried out in the passive region (−0.10–1.10 V) where the rate of corro-

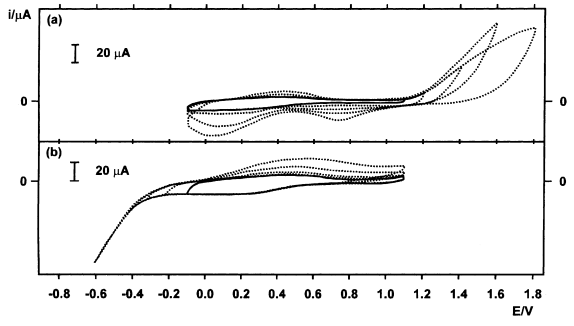

Fig. 4. Potential window-opening study (into anodic- and cathodic directions, respectively) of the disk-shaped austenitic stainless steel in the model solution. Scan rate 25 mV s^{-1}.

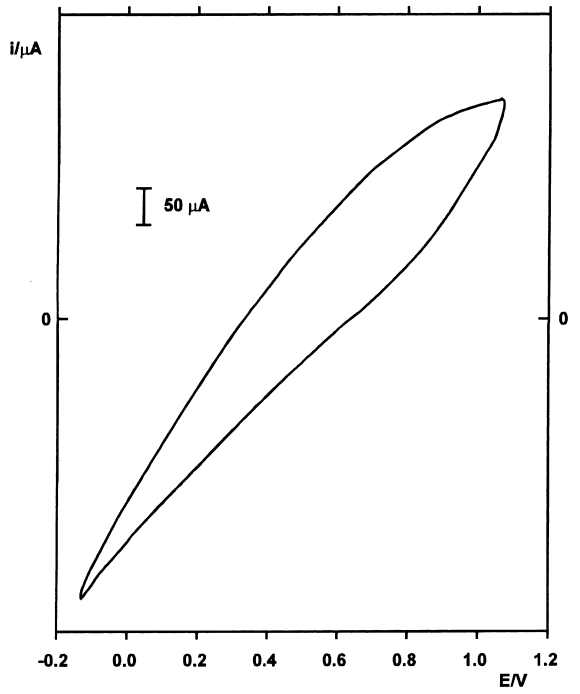

Fig. 5. Cyclic voltammogram of the disk-shaped magnetite-covered carbon steel in the model solution. Scan rate 25 mV s^{-1}.

sion and the amount of corrosion products dissolving into the solution phase can be kept low enough.

Voltammetric measurements with magnetite-covered carbon steel in the potential range of −0.1–1.1 V were also carried out in order to compare the CV results with those obtained for the passive austenitic stainless steel. As illustrated in Fig. 5, cyclic voltammogram of the magnetite-covered carbon steel differs completely from that of the austenitic stainless steel, i.e. an active dissolution of the carbon steel proceeds in the entire potential range, including the corrosion potential. Consequently, the sorption processes may take place not on a stable magnetite layer, but rather on a layer which changes continuously and is being covered by more and more corrosion products (metal-oxides and oxyhydroxides).

Finally, it has to be noted that addition of Ag (I) to the solution phase does not exert any significant effect on the shape of the voltammograms of neither austenitic nor carbon steel up to the silver concentration of 1×10^{-5} mol dm^{-3}.

3.2. In situ radiotracer study of silver deposition

In all the radiotracer experiments presented in this section the silver concentration was set to 1×10^{-6} mol dm^{-3}. As demonstrated by the relevant literature data [23,24] and Fig. 6 (this Pourbaix-diagram was calculated using the most up-to-date data available ([25] and references cited therein), in an aqueous solution containing 1×10^{-6} mol dm^{-3} Ag(I) at around pH = 7.7 silver occurs in +1 oxidation state. Ag^+ ions are stable in neutral or slightly alkaline solution due to the very moderate hydrolysis, but it is also known that they tend to form Ag_2O. In addition, it is of special importance to note that at pH = 7.7 (i.e. the pH of the model solution) the amount of hydrolysis products of silver (such as AgOH and $Ag(OH)_2^-$) is negligible [24]. Thus it can be concluded that under the above-mentioned experimental conditions the chemical form of Ag(I) in the solution phase may be ionic (Ag^+) and/or hardly soluble oxide (Ag_2O), from which the latter may exist as dissolved or colloid species. Upon polarization into positive direction the formation of various silver oxides with higher oxidation states (AgO, Ag_2O_3) cannot be excluded, as well as both the formation and deposition of atomic silver may take place in the lower potential region (see Fig. 6).

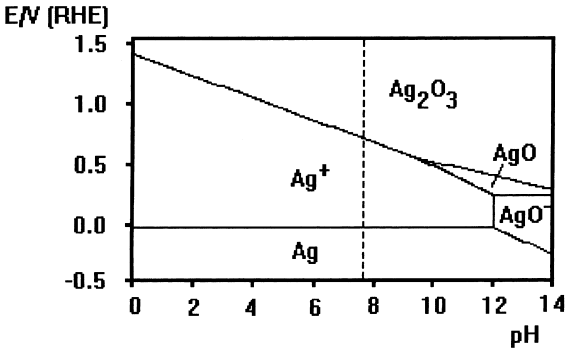

Fig. 6. Potential–pH diagram of Ag at room temperature for the concentration of 10^{-6} mol dm^{-3}. The vertical dashed line indicates pH = 7.7.

Fig. 7 shows the time dependence of silver accumulation on a disk-shaped sample of the austenitic stainless steel, measured by the in situ radiotracer thin gap technique in a model solution of the primary side coolant. A highly time and potential dependent sorption of silver species takes place on the smooth electrode surface, and no quasi-equilibrium surface excess of deposited silver is reached even after a period of 18 h. The fact that a surface excess of $\Gamma = 2 \times 10^{-9}$ mol cm^{-2} corresponds to one monolayer coverage of Ag^+ [26] provides evidence that only a limited part of the real surface area of the steel sample (less than 25%) is occupied by silver species. The surface excess concentration values at potentials more positive than the open-circuit potential are smaller (see inset in Fig. 7), indicating the significant effect of the electrode potential on the silver deposition processes.

Attempts were made to give a verification of our earlier findings [8,15,18–20] that a very thin dE/dx β-plastic scintillator is suitable for the measurement of the β-particles of β,γ-emitting isotopes (e.g. ^{110m}Ag, ^{60}Co)

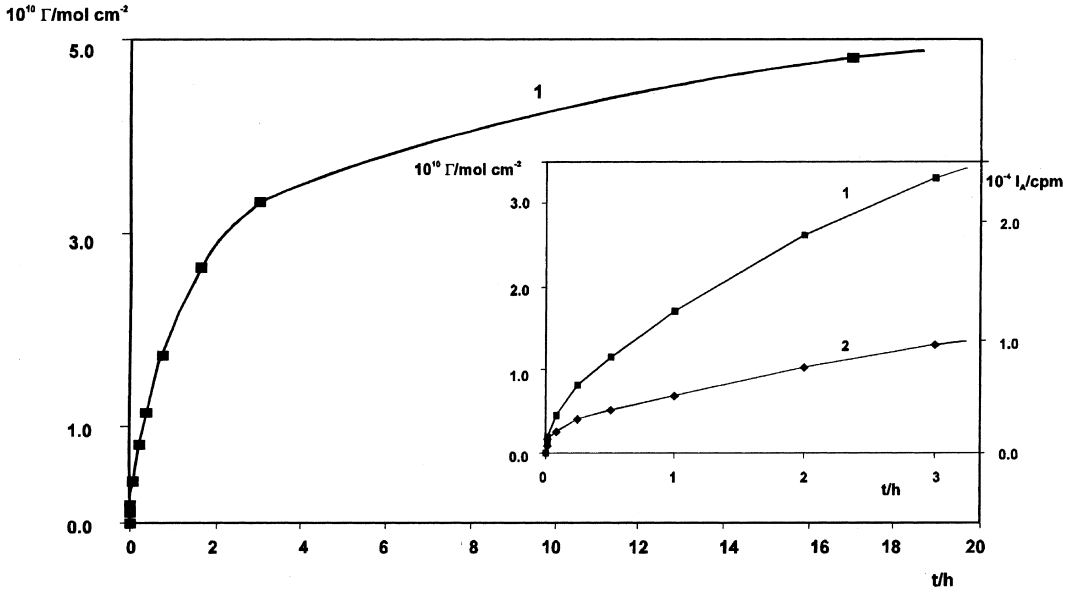

Fig. 7. Time dependence of the accumulation of silver labeled with ^{110m}Ag on the austenitic stainless steel in the model solution. In the inset, curves 1 and 2 show the accumulation at open-circuit potential ($E = 0.75$ V) and at 1.10 V, respectively.

with negligible contribution of the secondary radiations (γ- or characteristic X-rays, Compton electrons etc.). The latter statement is firmly supported by the multi-channel pulse-height spectra (Fig. 8) detected by an 100 μm thick β-plastic scintillator in the course of the silver deposition on austenitic stainless steel as there was no spectrum alteration found. The energy spectra shown in Fig. 8. also reveal that the original expression (see Eq. (1)), derived from the fundamental interactions of pure β-radiation, is valid for the calculation of the surface excess concentration of silver deposits labeled with ^{110m}Ag.

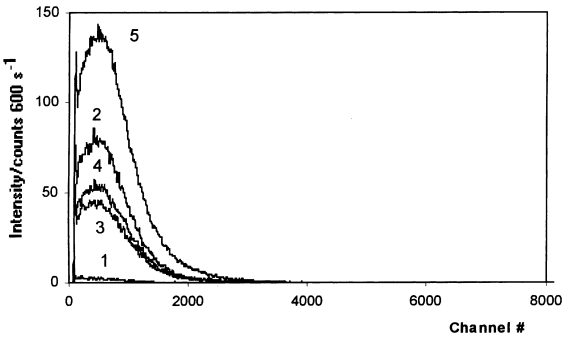

Fig. 8. Multi-channel pulse-height spectra of ^{110m}Ag measured by 0.1 mm thick β-plastic scintillator. The spectra were recorded during the time dependence measurement shown in Fig. 7; the measuring live time was 600 s. Arabic numbers besides the curves refer to: (1) environmental background, (2) solution background, (3) the 'gap', i.e., no adsorption occurs, (4) after 2 h of contamination, (5) after 17 h of contamination.

The predominant role of the electrode potential in the silver accumulation on austenitic stainless steel is highly supported by the Γ vs. E profiles presented in Fig. 9. Fig. 9(a) shows the cyclic voltammetry of the stainless steel in a borate buffer solution with and without silver ions. This cyclic voltammogram is essentially the same with those presented in Fig. 4, giving a further indication of the passive feature of the steel surface over a wide potential range both in the absence and in the presence of silver ions. Fig. 9(b) reveals a considerable decrease in Γ values at more anodic potentials than the open-circuit potential (curve 1). On the other hand, a potential shift into cathodic direction results in a significant increase in the surface excess concentration of silver (curve 1' in Fig. 9(b) and Fig. 9(c)). In accordance, *at potentials more negative than the open-circuit (corrosion) potential the cathodic current density is higher, too* (see Fig. 9(a)).

In the course of the slow surface transformation processes occurring in the passive region not only adsorption onto the surface, but a strong build-up of silver species into the passive oxide-layer of the austenitic stainless steel takes place. This assumption is strongly supported by the results of the exchange of the labeled silver accumulated on stainless steel (Fig. 10). In the mobility experiments great excess of inactive silver (10^{-4} mol dm^{-3}) was added to the solution phase or the boric acid concentration was elevated from 3 to 13 g dm^{-3}. As may be seen from the results in Fig. 10, part of the adsorbed species can be mobilized during a relatively short

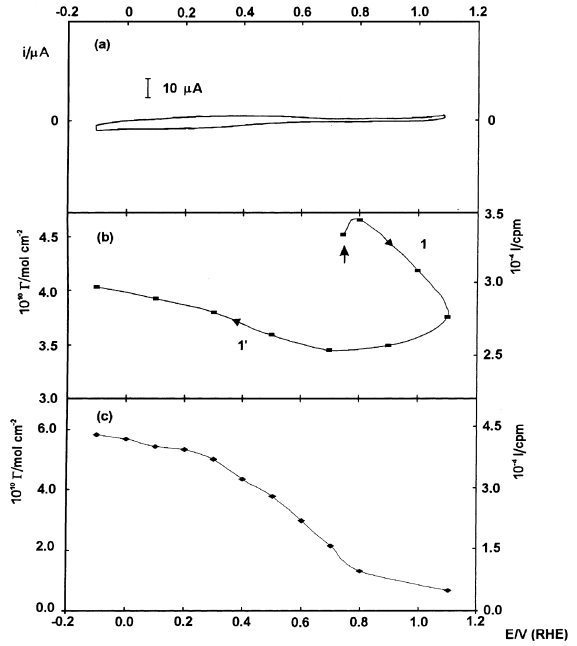

Fig. 9. (a) Cyclic voltammetry of disk-shaped austenitic stainless steel electrode in the model solution. Scan rate 10 mV s^{-1}. (b) Potential dependence of the adsorption of silver labeled with ^{110m}Ag on stainless steel in the model solution (curves 1 and 1', positive- and negative-direction plots, respectively). Arrow pointing upwards indicates the open-circuit potential. The experiment was carried out in continuous polarization mode, waiting for 30 min at each potential before obtaining intensity values. (c) Potential dependence of the adsorption of silver labeled with ^{110m}Ag on stainless steel in the model solution. The electrode was polarized into cathodic direction starting from 1.10 V. Other experimental conditions are as above.

period; however, following this zone the exchange rate slows down to a very low value, i.e., the completion of the exchange does not take place even after a period of several hours. From these observations it can be concluded that majority of the deposited silver is strongly bonded to the passive layer formed on austenitic stainless steel. The above implications are in accordance with the results obtained by XPS studies of the passive film.

In the light of the above results, a fundamental issue which emerges is how one can interpret the strong and potential dependent build-up of silver species. The substantial difference in the sorption behavior of Ag^+ and Ag_2O species, present in the solution phase, is expected to cause dissimilar accumulation at steel surfaces. The plausible contamination processes are schematically depicted in Fig. 11. In the present case, it is probable that *on the stainless steel surface a deposition process owing to the cementation of Ag^+ ions rather than the accumulation of Ag_2O prevails over the contamination phenomena*. During the cementation the dissolution of a metallic component of the passive steel surface is coupled with the reduction of silver ions to yield surface oxide-layer contaminated in depth with metallic silver. (An experimental evidence of the latter statement is given in Section 3.3.)

Furthermore, it can easily be understood that adsorption behavior of Ag(I) present in the solution at very low concentration ($c \leqslant 1\times10^{-6}$ mol dm^{-3}) is decisively dependent on its aqueous chemistry, as well as on the nature of the adsorbent. In neutral and slightly alkaline pH medium Ag^+ ions are very sensitive to oxidation by O_2 traces in the solution. Moreover, experiments performed with $Fe(OH)_3$ [27,28] in solution containing 1×10^{-7} mol dm^{-3} Ag(I) give an indication that hydrous iron oxide surfaces may also catalyze the formation of Ag(I) oxide. Assuming that corrosion products formed on magnetite-covered carbon steel indeed increase the relative amount of silver(I) oxide (Ag_2O) in the solution, the time and potential dependences of Ag(I) accumulation on magnetite-covered carbon steel are expected to vary significantly from that on austenitic stainless steel due not only to the differences in the nature and composition of steel surfaces, but also to the changes in the

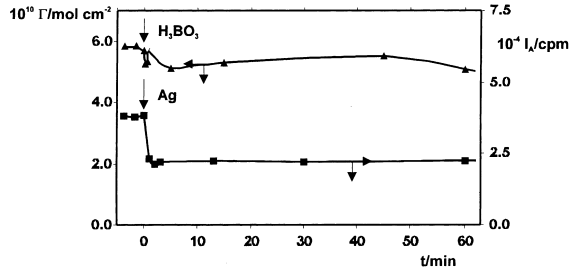

Fig. 10. Study of the mobility of radiolabeled Ag adsorbed on austenitic stainless steel by the addition of the great excess of inactive silver into the solution phase and the elevation of boric acid concentration from 3 to 13 g dm^{-3}. Arrows indicate the moment of addition.

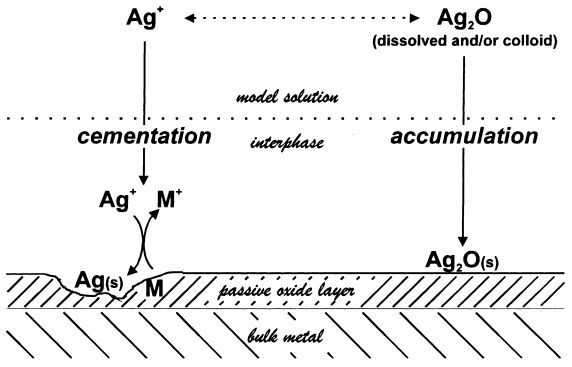

Fig. 11. Scheme of silver accumulation at austenitic stainless steel surfaces.

chemical state of the majority of Ag(I) species to be adsorbed.

In accordance with the above expectations, comparative studies of silver contamination on magnetite-covered carbon steel (Figs. 12–14) clearly demonstrate that the carbon steel exhibits markedly different sorption behaviors than the austenitic one under identical experimental conditions. As it has been revealed in Section 3.2, an active dissolution of magnetite-covered carbon steel takes place in the potential region of −0.10–1.10 V; therefore, one may expect enormous silver accumulation via some cementation processes. In contrast, the extent of silver sorption in this case is one order of magnitude lower than on the austenitic stainless steel as reflected by the Γ vs time curve in Fig. 12. It should, however, be noted that this curve does not show equilibrium feature. Furthermore, as it may be seen from Fig. 13, the surface excess concentration values do not depend on the applied potential in the potential region of −0.10–1.10 V. The surprising sorption feature shown in Figs. 12 and 13 is indicative of a distinctly different mode of the surface binding of silver species. At this stage in our studies, it is impossible to clarify the exact mechanism of the silver accumulation; however, in accordance with the data in [27,28], it is probable that the various corrosion products (hydroxides and oxyhydroxides) dissolved from the carbon steel into the solution phase promotes the formation of silver(I) oxide (Ag_2O). Even though the Ag(I) oxides exhibit low solubility, they cannot accumulate in great extent on a steel surface undergoing intensive chemical and structural transformation. Nevertheless, the labeled silver species bound to the carbon steel surface were almost impossible to exchange by addition of 10^{-4} mol dm^{-3} inactive Ag(I) to the solution phase (Fig. 14). It is interesting to note that the elevation of boric acid concentration from 3 to 13 g dm^{-3} resulted in a slightly higher extent of silver sorption. The latter effect presented in Fig. 14 is most likely due to the pH drop (from 7.7 down to 4.8) in the solution which assists the re-formation of Ag^+ ions.

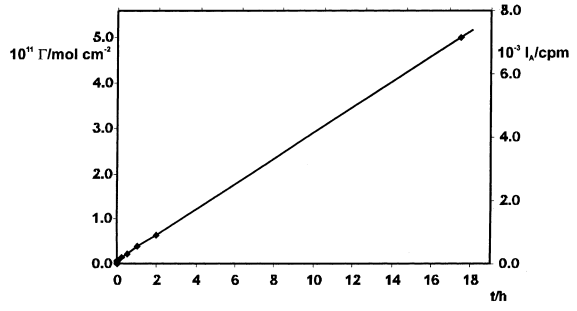

Fig. 12. Time dependence of the accumulation of silver labeled with ^{110m}Ag on the magnetite-covered carbon steel in the model solution at open-circuit potential ($E = 0.39$ V).

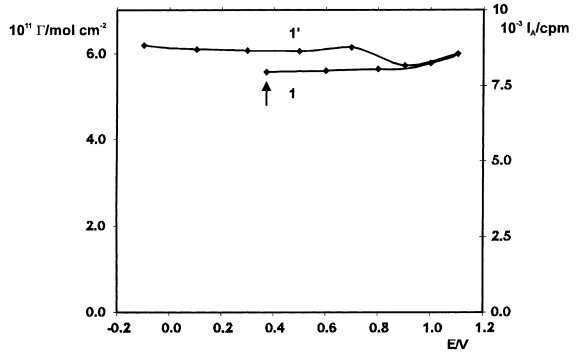

Fig. 13. Potential dependence of the adsorption of silver labeled with ^{110m}Ag on magnetite-covered carbon steel in the model solution (curves 1 and 1', positive- and negative-direction plots, respectively). Arrow pointing upwards indicates open-circuit potential. The experiment was carried out in continuous polarization mode, waiting for 30 min at each potential before obtaining intensity values.

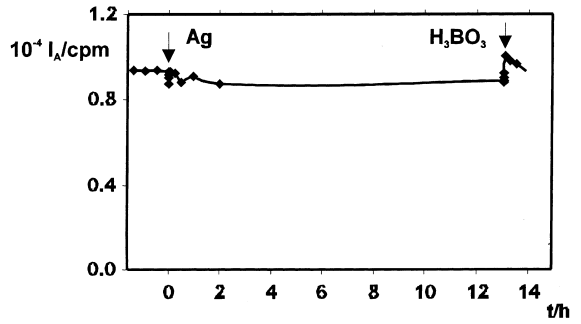

Fig. 14. Study of the mobility of radiolabeled Ag adsorbed on magnetite-covered carbon steel by the addition of great excess of inactive silver into the solution phase and the elevation of boric acid concentration from 3 to 13 g dm^{-3}. Arrows indicate the moment of addition.

3.3. Characterization of silver deposits on austenitic stainless steel by XPS

In order to characterize the depth distribution and chemical state of silver species deposited onto the passive layers of austenitic stainless steel type 08X18H10T, comparative studies were made by X-ray photoelectron spectroscopy (XPS). In these experiments three steel samples were brought into contact with model solution containing 10^{-6} mol dm^{-3} unlabeled Ag(I) for 1 and 20 h at open-circuit potential, and for 4 h at −0.1 V. Other aspects of the pretreatment were detailed in the Section 2.

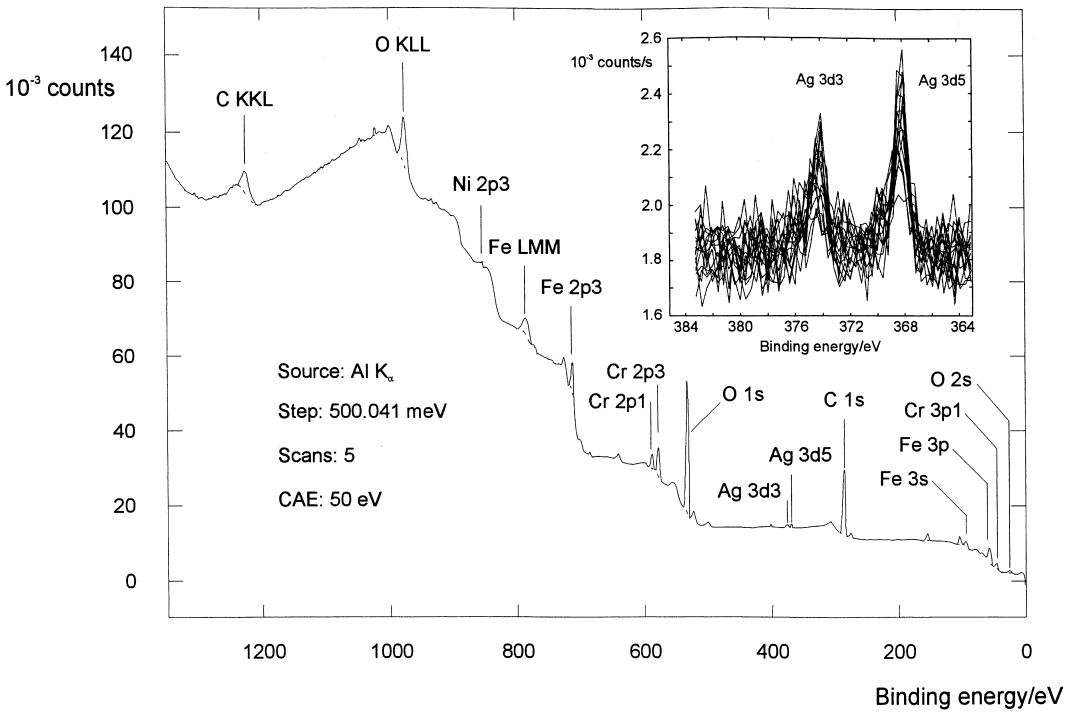

Fig. 15. Wide XPS scan of austenitic stainless steel sample polarized to −0.1 V for 4 h in model solution containing 10^{-6} mol dm^{-3} Ag(I). In the inset the Ag 3d3 and Ag 3d5 peaks can be seen.

The silver species deposited on the surface at open-circuit potential even after a period of 20 h could not be detected by the XPS. Silver was only detectable on the steel sample polarized at −0.10 V (Fig. 15); however, its measured amount in the film was very low, about 0.2% expressed in atomic concentration (Fig. 16). Comparing the detection limit of silver species by the XPS with the fact that less than 25% of the monolayer coverage provides a well-measurable intensity surplus by the radiotracer thin gap technique (see Fig. 7), the application of the in situ radiotracer methods in the studies of submonolayer Ag coverages seems to be full of potentialities.

As may be seen from Figs. 15 and 16, besides the detection of the depth profiles for carbon, iron, oxygen and chromium, the very aim of our XPS studies was to determine the chemical state and depth distribution of silver in the passive layer. The thickness of the passive film was found to be about 2 nm, assuming that 1 min sputtering removes 1 nm from the layer. The center of the Ag 3d5 peak in Fig. 15 is located at 368.5 eV (in binding energy) which is very close to that of metallic silver (just above 368.1 eV). According to [29] the peaks of silver oxides are situated definitely below this value (367.4–368.0 eV), so the accumulated silver is most likely in metallic state. As can be seen from the Ag depth profile in Fig. 16, silver occurs in the entire passive layer; neither its amount, nor the location of its peaks change with the depth. All these results fortify our assumptions that the silver sorption on austenitic stainless steel type

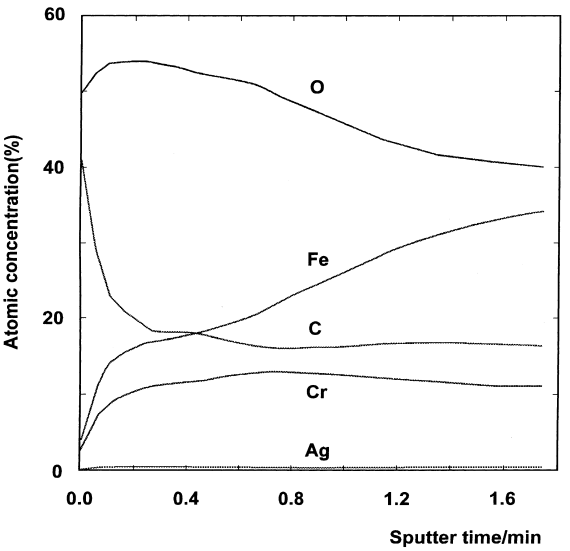

Fig. 16. XPS depth profiles for oxygen, carbon, chromium, iron and silver in the passive layer of the austenitic stainless steel (1 min sputtering corresponds to ~1 nm thickness).

08X18H10T mainly proceeds via some cementation processes to yield passive oxide-layer contaminated in depth with metallic Ag.

4. Conclusion

The austenitic stainless steel type 08X18H10T exhibits passive behavior in the potential region of −0.10–1.10 V vs. RHE. In this range the corrosion rate is retarded and the amount of corrosion products dissolved into the solution is low. It is to be noted that the passivity of stainless steel in the above wide potential region provides favorable conditions for normal industrial application in several aspects (such as corrosion, corrosion-prevention, radioactive contamination and decontamination). In the same potential region the magnetite-covered carbon steel corrodes heavily, therefore its application has to be avoided as much as possible.

^{110m}Ag contamination on austenitic stainless steel surfaces can take place in oxide (Ag_2O) and/or ionic (Ag^+) forms, from which the deposition of Ag^+ ions is predominant. Since the sorption of silver ions is potential dependent, the extent of ^{110m}Ag contamination can be minimized by polarizing the surface to the most positive value ($E = 1.10$ V) in the passive range. At this potential value the corrosion current also exhibits minimum feature. Silver accumulation on magnetite-covered carbon steel surfaces is one order of magnitude lower than on austenitic stainless steel ones owing to the facts that (i) the formation of silver oxide is most likely promoted by the corrosion products, and (ii) the steel surface undergoes intensive chemical and structural transformation.

The XPS results strongly support (i) the unique sensitivity of the in situ thin gap radiotracer method in the studies of submonolayer Ag coverages, and (ii) the predominant role of the cementation processes in the ^{110m}Ag contamination at austenitic stainless steel surfaces. Moreover, the obtained depth profile gives an evidence about the embedding of metallic silver into the entire passive layer. Consequently, any effective silver decontamination should necessarily be accompanied with the removal of the passive layer, too. To avoid ^{110m}Ag contamination as much as possible, the dissolution rate of the steel has to be minimized, preferably by the polarization of the sample to 1.10 V vs RHE.

Acknowledgements

This work was supported by the Paks NPP Co. Ltd. (Paks, Hungary), the Ministry of Education of Hungary (Grant No. 0789/97), the Hungarian Science Foundation (OTKA Grant No. F015695) and the FRD of South Africa.

References

[1] D.H. Lister, Water Chem. of Nucl. React. Systems. 6. BNES, London, 1992, p. 49.
[2] G.C.W. Comley, Prog. Nucl. Energy 16 (1985) 41.
[3] A.P. Murray, Nucl. Technol. 74 (1986) 324.
[4] G.L. Horváth, P. Ormai, T. Pintér, I.C. Szabó, Kernenergie 30 (1987) 38.
[5] Von H. Hepp, H. Generlich, E. Jaensch, Kraftwerkstechnik 59 (1979) 158.
[6] Second International Seminar on Primary and Secondary Side Water Chemistry of Nuclear Power Plants, Proceedings, Balatonfüred, Hungary, 19-23 September 1995.
[7] Third International Seminar on Primary and Secondary Side Water Chemistry of Nuclear Power Plants, Proceedings, Balatonfüred, Hungary, 16–20 September 1997.
[8] K. Varga, G. Hirschberg, P. Baradlai, M. Nagy, in: E. Matijević (Ed.), Surface and Colloid Science. Plenum, New York, vol. 16, in press.
[9] V.E. Kazarinov, V.N. Andreev, in: E. Yeager, J.O.'M. Bockris, B. Conway, S. Sarangapani (Eds.), Comprehensive Treatise of Electrochemistry, Plenum, New York, 1984, vol. 9, p. 393.
[10] A. Wieckowski, in: R.E. White, J.O'M. Bockris, B. Conway (Eds.), Modern Aspects of Electrochemistry, Plenum, New York, 1990, vol. 21, p. 65.
[11] E.K. Krauskopf, A. Wieckowski, in: J. Lipkowski, R.P. Ross (Eds.), Frontiers of Electrochemistry. VCH Publishers, New York, 1992, vol. 1, p. 119.
[12] G. Horányi, Rev. Anal. Chem. 14 (1995) 1.
[13] M. Nagy, P. Baradlai, L. Tomcsányi, K. Varga, ACH-Models in Chemistry, 132 (1995) 561.
[14] K. Varga, P. Baradlai, W.O. Barnard, J.H. Potgieter, P. Halmos, Magy. Kém. Folyóirat 102 (1996) 143.
[15] G. Hirschberg, Z. Németh, K. Varga, J. Electroanal. Chem. 456 (1998) 171.
[16] V.E. Kazarinov, Electrokhimiya 2 (1966) 1170.
[17] V.E. Kazarinov, G.J. Tysyachnaya, V.N. Andreev, J. Electroanal. Chem. 65 (1975) 391.
[18] K. Varga, M. Nagy, Magy. Kém. Folyóirat. 103 (7) (1997) 297.
[19] G. Hirschberg, K. Varga, Meeting Abstract Volume, Joint International Meeting of the ECS and ISE, Paris, France, 30 August–5 September 1997. pp. 1175–1176.
[20] G. Hirschberg, K. Varga, P. Baradlai, Z. Németh, J. Schunk, P. Tilky, in: Proceedings of the Third International Seminar on Primary and Secondary Side Water Chemistry of Nuclear Power Plants, Balatonfüred, Hungary, 16–20 September 1997.
[21] N. Ramasubramanian, N. Preocanin, R.D. Davidson, J. Electrochem. Soc. 132 (1985) 793.
[22] A.E. Thomas, Y.E. Sung, M. Gamboa-Aldeco, K. Franaszczuk, A. Wieckowski, J. Electrochem. Soc. 142 (1995) 476.
[23] M. Pourbaix, Atlas of Electrochemical Equilibria in Aqueous Solutions, Pergamon, Oxford, 1966.

[24] C.F. Baes, R.E. Mesmer, The Hydrolysis of Cations, Wiley, New York, 1976.
[25] T. Kristóf, T. Salamon, Cs. Mihálykó, Hung. J. Indust. Chem. 21 (1993) 75.
[26] D.M. Kolb, in: Gerischer, H., Tobias, C.W. (Eds.), Advances in Electrochemistry and Electrochemical Engineering, Wiley, New York, 1978, vol. 11, p. 127.
[27] S. Music, M. Ristic, J. Radioanal. Nucl. Chem. Articles 120 (1988) 289.
[28] S. Music, Isotopenpraxis 21 (1985) 143.
[29] J. Chastain, R.C. King (Eds.), Handbook of X-ray Photoelectron Spectroscopy. Physical Electronics, Minnesota, 1995.